Multicomponent deblending of marine data using a pattern-based approach

Joseph Jennings, Robert Clapp, Biondo Biondi and Shuki Ronen, Stanford University*

SUMMARY

We present the theory and initial results for deblending multicomponent simultaneous source data using a pattern-based approach based on multidimensional prediction-error filters (PEFs). In using this pattern-based approach, we provide a method for PEF estimation that makes use of the directional information recorded on the geophone components in order to improve the source separation on the hydrophone. We provide synthetic numerical examples and an example from a FreeCable^{TM} data set that demonstrate that using PEFs estimated on all data components results in better separation than using only the hydrophone component.

INTRODUCTION

Simultaneous source deblending

In traditional seismic acquisition, a wait time is introduced between shots to reduce the possibility of overlap. Simultaneous source acquisition removes this constraint therefore introducing overlap between shots and reduces the total survey time (Beasley et al., 1998). In order to obtain high-quality subsurface images, this overlap must be properly dealt with in processing/imaging simultaneous source ("blended") data.

Pattern-based approach using PEFs

One way to view these blended data is that in the common-shot domain the blended data consist of signal and a sum of coherent noise sources (Berkhout, 2008). Viewing the deblending problem in this way helps us to think of using methods known as pattern-based approaches used for separating signal and coherent noise (Abma, 1995). Pattern-based approaches separate signal and noise using the fact that the multidimensional spectra of the signal and noise differ. These approaches have been successfully used in multiple removal, ground-roll attenuation and other coherent noise removal applications (Manin and Spitz, 1995; Brown et al., 2001; Guitton, 2005). In spite of their success, perhaps the most challenging part of working with pattern-based approaches is that they require a model of the patterns of the signal and the noise. With these models, prediction-error filters (PEFs) are then estimated and used then as proxies for the multidimensional spectra of the signal and noise. While for some coherent noise removal problems, there exist systematic methods for obtaining these signal and noise models, no such method exists for modeling the interfering noise sources for the deblending problem. Because the focus of this work is on incorporating multicomponent data to improve a pattern-based approach, for all examples here we assume ideal models for both the signal and the noise.

Multicomponent data

While these pattern-based approaches typically use PEFs estimated in the time-offset ($t - x$) space, incorporating patterns from the geophone components of multicomponent data has the potential to improve the signal and noise separation. Unlike the hydrophone component which is an omni-directional sensor, the geophone components offer directional (polarity) information about the coherent noise. This is especially true for blended data for which the horizontal geophone components will provide useful patterns for the interfering source depending on the relative positions of the two sources (Jennings and Ronen, 2017).

In order to leverage the directional information offered by the multicomponent data typically acquired during marine simultaneous source surveys, we extend the pattern-based approach to incorporate multicomponent data and use this additonal information to improve the deblending on the hydrophone. We estimate non-stationary PEFs on the hydrophone and geophone components simultaneously, providing patterns over time and offset and the directional information from the multicomponent data. On a 1D synthetic example, we show that using the geophone data allows for separation of signal and noise where it would be otherwise impossible using only the hydrophone data. In 2D, we show that using non-stationary PEFs estimated on the multicomponent data provides faster convergence for deblending blended data. Lastly, we demonstrate on a FreeCable^{TM} dataset acquired in the Mediterranean sea (Haumonté et al., 2016) that the usage of PEFs estimated on multicomponent data provides better source separation on the hydrophone component than using the hydrophone alone.

THEORY

For a simple case in which the blended data consists of just two shots, the blended data can be expressed as

$$\tilde{\mathbf{d}} = \mathbf{d}_1^s + \mathbf{d}_2^s, \tag{1}$$

where $\tilde{\mathbf{d}}$ is the recorded blended data, $\mathbf{d}_1^s$ is the shot of interest $\mathbf{d}_2^s$ is the interfering shot (note that while all derivations here are done assuming just two shots, the theory extends to more than just two shots). The superscript ^{s} indicates that these shots may be time-shifted. The goal of simultaneous source deblending is to recover both $\mathbf{d}_1^s$ and $\mathbf{d}_2^s$ from $\widetilde{\mathbf{d}}$. We can write this mathematically as the minimization of an objective function of the form

$$J(\mathbf{d}_1^s, \mathbf{d}_2^s) = \frac{1}{2}||\mathbf{d}_1^s + \mathbf{d}_1^s - \tilde{\mathbf{d}}||_2^2. \tag{2}$$

Directly minimizing equation 2 will not result in a separated $\mathbf{d}_1^s$ and $\mathbf{d}_2^s$ due to the fact that it is ill-posed. We need additional constraints on $\mathbf{d}_1^s$ and $\mathbf{d}_2^s$ in order to deblend the data. A pattern-based approach will provide constraints derived from the multidimensional spectra of $\mathbf{d}_1^s$ and $\mathbf{d}_2^s$. Obtaining the multidimensional spectra of the data requires estimating non-stationary PEFs on models of both $\mathbf{d}_1^s$ and $\mathbf{d}_2^s$ which we denote as $\hat{\mathbf{d}}_1^s$ and $\hat{\mathbf{d}}_2^s$. This process of PEF estimation can be written as the following regressions

$$\mathbf{0} \approx \mathbf{r} = \hat{\mathbf{D}}_1^s \mathbf{f}_1, \quad \mathbf{0} \approx \mathbf{r} = \hat{\mathbf{D}}_2^s \mathbf{f}_2,$$

10.1190/segam2018-2996253.1

where $\hat{\mathbf{D}}_1^s\mathbf{f}_1$ and $\hat{\mathbf{D}}_2^s\mathbf{f}_2$ indicates the convolution of $\hat{\mathbf{d}}_1^s$ and $\hat{\mathbf{d}}_2^s$ with the unknown filter coefficients $\mathbf{f}_1$ and $\mathbf{f}_2$ respectively and $\mathbf{r}_1$ and $\mathbf{r}_2$ are the prediction-error residuals for $\mathbf{f}_1$ and $\mathbf{f}_2$ respectively. These fitting goals essentially state that we desire to find filters $\mathbf{f}_1$ and $\mathbf{f}_2$ that can optimally predict our data. Note that in order for these filters to remain PEFs, we require that the first coefficient be set to unity. To enforce this, we introduce a masking matrix during the optimization for the filter coefficients that allows all other coefficients to be adjustable except for the first sample. Upon solving these regression equations, we obtain non-stationary multidimensional PEFs that contain the approximate inverse spectra of $\hat{\mathbf{d}}_1^s$ and $\hat{\mathbf{d}}_2^s$ (Claerbout, 2014).

With these PEFs, we then form convolution operators $\mathbf{F}_1$ and $\mathbf{F}_2$ and use these operators as constraining terms in the following objective function to obtain estimates of $\mathbf{d}_1$ and $\mathbf{d}_2$

$$J(\mathbf{d}_1^s, \mathbf{d}_2^s) = \frac{1}{2}||\mathbf{d}_1^s + \mathbf{d}_2^s - \tilde{\mathbf{d}}||_2^2 + \frac{1}{2}||\mathbf{F}_1\mathbf{d}_1^s||_2^2 + \frac{1}{2}||\mathbf{F}_2\mathbf{d}_2^s||_2^2. \quad (3)$$

Note that the first term in equation 3 is the same as stated in equation 2 and attempts to minimize the error between our estimate for the blended data and the true blended data. The additional two terms act as constraints in order to enforce the separation of the shots. Due to the fact that $\mathbf{A}_1$ and $\mathbf{A}_2$ contain the inverse spectra of $\hat{\mathbf{d}}_1^s$ and $\hat{\mathbf{d}}_2^s$ respectively they effectively regularize the estimated $\mathbf{d}_1^s$ and $\mathbf{d}_2^s$ so that they contain the spectra of $\hat{\mathbf{d}}_1^s$ and $\hat{\mathbf{d}}_2^s$ respectively.

PEFs estimated on multicomponent data

One key factor in the success of the pattern-based approach just described is that it will perform better for higher dimensional data. This is because while some events may not be separable in temporal frequency, their spectra may differ greatly in spatial frequency (dip). Additionally, we record multicomponent data that contain information on the polarity of certain events which provide even more information in order to differentiate the signal from the noise. In order to capture this information, we make the assumption that one component can be treated as a linear combination of the other. We do this by creating a multichannel filter with multiple inputs (the different components) and a single output (the prediction-error on the hydrophone). For example, if we choose to estimate a PEF on the vertical and hydrophone components, the filter will attempt to use samples from the vertical component to make a prediction on the hydrophone component. By making this assumption the PEF is able to capture directional patterns contained on the geophone components and we show that this improves deblending of the hydrophone component.

RESULTS

Synthetic example in 1D

We first tested our pattern-based approach using PEFs estimated on multicomponent data on a simple synthetic example that contained the blended direct arrivals of two events. In order to test the use of the directional information recorded on the horizontal components, we positioned one source crossline to the line of receivers and the other inline with the line of receivers. For our homogeneous model, this resulted in two direct arrivals that are highly polarized on the horizontal components. Figure 1 shows the multicomponent blended data. Note that because of the polarization of the direct arrival, the Y-component does not even appear blended (Figure 1a). It is this information that we desire that the PEF can use from the multicomponent data to improve the deblending of the shots. To test this, we first extracted one trace from the location of the blue line shown on the blended data in Figure 1. We selected this trace as both the signal and noise have 100% overlap, but exhibit different polarization on the horizontal components. Figure 2 shows the results of the signal and noise separation of just the single trace. The top row shows that while using just the hydrophone data resulted in an inverted $\mathbf{d}_1^s$ and $\mathbf{d}_2^s$ that satisfy equation 1, they are not the correct signal and noise as is evident by the mismatch between the estimated (red curve) and true (blue curve) data. This was expected, as due to the 100% overlap of the signal and noise, more information is required for separation. The PEF estimated on the multicomponent data uses the different polarizations to separate the single traces of $\mathbf{d}_1^s$ and $\mathbf{d}_2^s$.

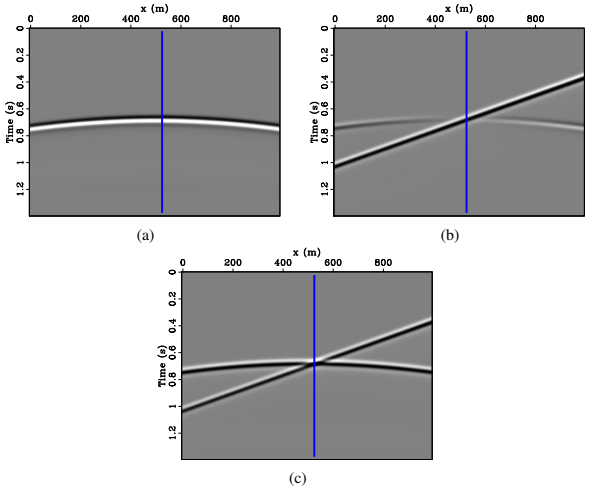

Figure 1: Blended direct arrivals from a homogeneous 2D model. (a) Y-component of particle velocity, (b) X-component of particle velocity and (c) hydrophone component. Note that while the hydrophone contains both events, because of the polarized nature of these direct arrivals, the Y-component did not record the inline shot and the cross line shot is much weaker on the X-component. The blue line indicates the position of the trace for which we performed the 1D example (Figure 2).

Synthetic example in 2D

We then tested our approach using all traces seen in Figure 1. We found that while both single and multicomponent approaches were able to deblend the shots, using the multicomponent approach exhibited faster convergence. Figure 3 shows the result of the deblending inversion after 20 iterations of minimizing equation 3 using a conjugate gradient solver. Figure 4 shows the comparison of the model residual for both $\mathbf{d}_1^s$ and $\mathbf{d}_2^s$.

Field data example: FreeCable^{TM} data from the Mediterranean sea

We then tested our approach on a field data set that was ac-

10.1190/segam2018-2996253.1

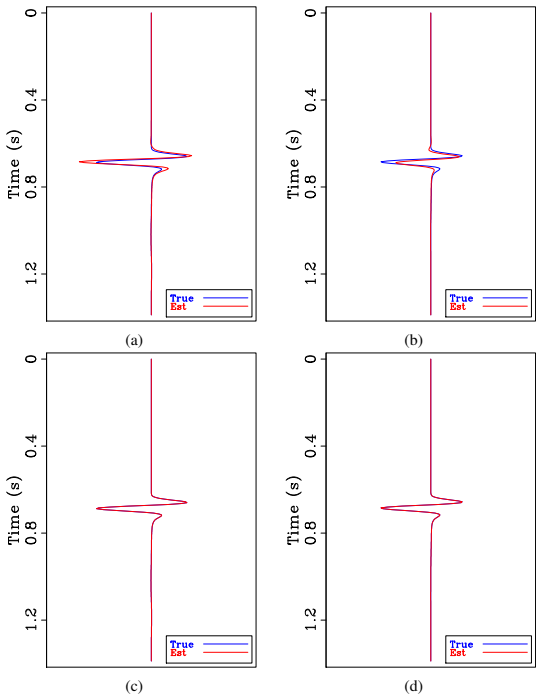

Figure 2: Results of the signal and noise separation of one trace of the blended data (the blue line in Figure 1) using just the hydrophone data (top row) and using all data components (bottom row). Panels (a) and (c) show the comparison of the estimated (red curve) and true (blue curve) $\mathbf{d}_1^s$. Similarly panels (b) and (d) show the same comparison but for $\mathbf{d}_2^s$. Note that as expected, there is a mismatch between the true and estimated $\mathbf{d}_s^1$ and $\mathbf{d}_s^2$ for panels (a) and (b) because of the 100% overlap in using just the hydrophone data. However, using the horizontal components (panels (c) and (d)) allows for good recovery of $\mathbf{d}_1^s$ and $\mathbf{d}_2^s$ (the red and blue curves completely overlap).

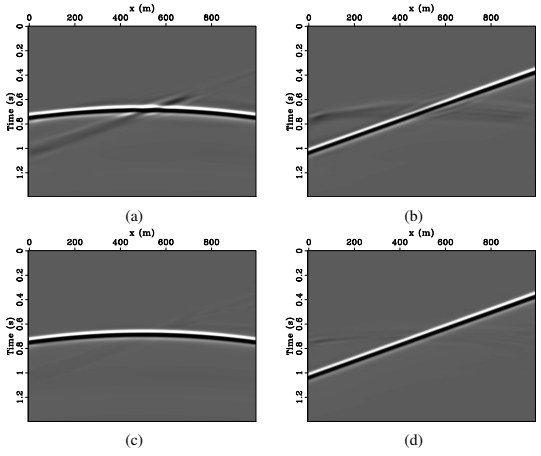

Figure 3: Top row: deblending results after 20 iterations of inversion (equation 3) using only hydrophone component. Bottom row: results of hydrophone deblending after 20 iterations using multicomponent data.

quired in 2014 by Kietta in the Mediterranean sea (Haumonté et al., 2016). These data were acquired with a FreeCable^{TM} technology that consists of a cable equipped with four component receivers that is suspended in the water column. This acquisition setup allows for an ideal test of our PEFs estimated on multicomponent data as the receivers have nearly perfect coupling to the medium and the data also are free of elastic wave propagation effects. As these data were not blended, we synthetically blended them assuming two source vessels. Figure 5 shows the acquisition geometry for one blended shot and Figure 6a shows the resulting blended data recorded on the hydrophone. We then deblended these shots using a pattern-based approach. Figure 6b shows the deblended crossline shot using just the hydrophone component to perform the deblending and Figure 6c shows the same result but used the horizontal components in addition to the hydrophone component to deblend the data. When comparing Figures 6b and 6c with the unblended data shown in Figure 6d, it is clear that using the horizontal components in addition to the hydrophone component removed more of the interfering shot. This is also evident in Figure 7 which shows the differences between the deblended and unblended data for both single (Figure 7a) and multicomponent approaches (Figure 7b).

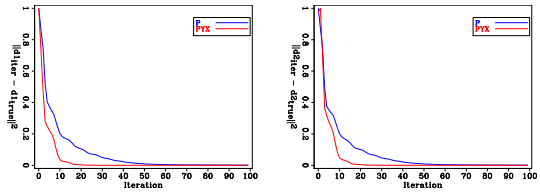

Figure 4: Comparison of hydrophone component model residuals ($||\mathbf{d}^s_{\text{true}} - \mathbf{d}^s_{\text{iter}}||_2^2$) for (a) the separated inline shot and (b) the separated cross line shot. Blue curve curve represents single component convergence. Red curve indicates multicomponent convergence. The use of all data components allows for faster convergence to the deblended data.

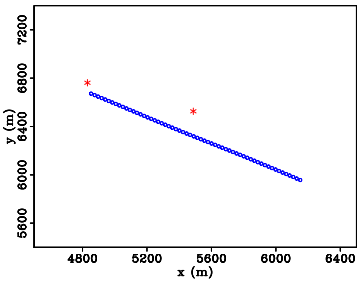

Figure 5: The locations of the two sources (red stars) and receivers (blue circles) that resulted in the blended data shown in Figure 7a. Note that because one shot is in the inline direction, and the other the cross line direction the polarization information recorded on the horizontal components can be used for improving the source separation.

10.1190/segam2018-2996253.1

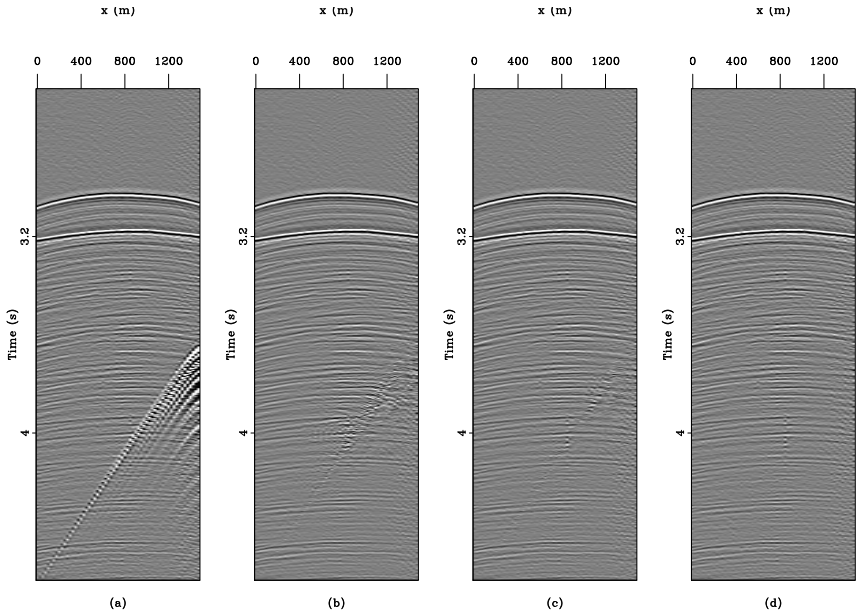

Figure 6: Deblending of the Mediterranean sea data. (a) The blended data, where the direct arrival resulted from the inline shot and the reflections resulted from the cross-line shot. (b) The result of deblending using only the hydrophone component. Note that significant residual interference remains. (c) The deblended data obtained using both the hydrophone and horizontal components. While residual interference remains, it has been significantly reduced when compared to the single component approach. (d) The unblended data included for comparison.

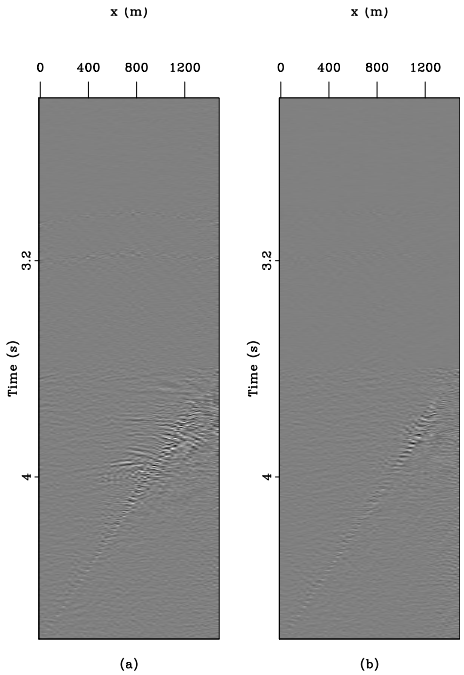

Figure 7: Differences between deblended and unblended data. (a) Difference between deblended data using just the hydrophone component and the unblended hydrophone data (difference between Figure 6b and Figure 6d). (b) Difference between deblended data using hydrophone and horizontal components and unblended data (difference between Figure 6c and Figure 6d).

Defining the signal to noise ratio (SNR) as follows,

$$\text{SNR} = \frac{||\mathbf{d}_0||_2^2}{||\mathbf{d}_0 - \mathbf{d}||_2^2} \tag{4}$$

where $\mathbf{d}_0$ is the unblended data and $\mathbf{d}$ is the deblended data, we find that using the hydrophone data alone results in an SNR of 11.65 dB (Figure 6b) and using the hydrophone and horizontal components gives an SNR of 16.17 dB (Figure 6c).

CONCLUSION

We extended the pattern-based approach for signal and noise separation to incorporate multicomponent data and applied it to the simultaneous source deblending problem. We showed that using the geophone components allowed for better separation of the hydrophone data on both synthetic and field data examples. Because the pattern-based approach requires models of the signal and noise, we used the signal and noise themselves for each of the examples shown. For future work, we plan to investigate the performance of both approaches in the absence of accurate signal and noise models. Additionally, we plan to investigate imposing additional sparsity constraints in order to take advantage of the success of sparse inversion techniques (Abma et al., 2015).

ACKNOWLEDGEMENTS

We thank Kietta for releasing the data to Stanford University, the affiliates of the Stanford Exploration Project for their support and the other students and professors at Stanford for their help and advice.

10.1190/segam2018-2996253.1

REFERENCES

Abma, R., D. Howe, M. Foster, I. Ahmed, M. Tanis, Q. Zhang, A. Arogunmati, and G. Alexander, 2015, Independent simultaneous source acquisition and processing: Geophysics, **80**, no. 6, WD37–WD44, https://doi.org/10.1190/geo2015-0078.1.

Abma, R., 1995, Least-squares separation of signal and noise with multidimensional filters: Ph.D. dissertation, Stanford University.

Beasley, C. J., R. E. Chamber, and Z. Jiang, 1998, A new look at simultaneous sources: 68th Annual International Meeting, SEG, Expanded Abstracts, 133–135, https://doi.org/10.1190/1.1820149.

Berkhout, A. J., 2008, Changing the mindset in seismic data acquisition: The Leading Edge, **27**, 924–938, https://doi.org/10.1190/1.2954035.

Brown, M., R. G. Clapp, and K. Marfurt, 2001, Predictive signal/noise separation of ground-roll-contaminated data: SEP-Report, **102**, 111–128.

Claerbout, J., 2014, Geophysical image estimation by example, lulu.com.

Guitton, A., 2005, Multiple attenuation in complex geology with a pattern-based approach: Geophysics, **70**, no. 5, V97–V107, https://doi.org/10.1190/1.1997369.

Haumonté, L., L. Velay, and M. Manin, 2016, In situ test results in the Mediterranean Sea with a novel marine seismic acquisition system (FreeCableTM): 86th Annual International Meeting, SEG, Expanded Abstracts, 51–55, https://doi.org/10.1190/segam2016-13865545.1.

Jennings, J., and S. Ronen, 2017, Simultaneous source deblending with the radiality and source-similarity attributes: 87th Annual International Meeting, SEG, Expanded Abstracts, 4909–4913, https://doi.org/10.1190/segam2017-17736410.1.

Manin, M., and S. Spitz, 1995, 3D attenuation of targeted multiples with a pattern recognition technique: 57th Annual International Meeting, EAGE, Extended Abstracts, B046.